ACS NANO

Cite This: ACS Nano 2018, 12, 7519−7528

www.acsnano.org

ARTICLE

Highly Effective Radioisotope Cancer Therapy with a Non-Therapeutic Isotope Delivered and Sensitized by Nanoscale Coordination Polymers

Yu Chao,[†] Chao Liang,[†] Yu Yang,[†] Guanglin Wang,[‡] Debabrata Maiti,[†] Longlong Tian,[†] Fei Wang,[§] Wei Pan,[∥] Song Wu,*[,§] Kai Yang,*[,‡] and Zhuang Liu*[,†]

[†]Institute of Functional Nano & Soft Materials (FUNSOM), Jiangsu Key Laboratory for Carbon-Based Functional Materials & Devices and [‡]State Key Laboratory of Radiation Medicine and Protection, School of Radiation Medicine and Protection & School for Radiological and Interdisciplinary Sciences (RAD-X), Collaborative Innovation Center of Radiation Medicine of Jiangsu Higher Education Institutions, Soochow University, Suzhou, Jiangsu 215123, China

[§]Institute of Urology of Shenzhen University, The Third Affiliated Hospital of Shenzhen University, Shenzhen Luohu Hospital Group, Shenzhen 518000, China

[∥]College of Chemistry, Chemical Engineering and Materials Science, Shandong Normal University, Jinan 250014, China

Supporting Information

ABSTRACT: **Nuclear medicine with radioisotopes is extremely useful for clinical cancer diagnosis, prognosis, and treatment. Herein, polyethylene glycol (PEG)-modified nanoscale coordination polymers (NCPs) composed of hafnium (Hf^{4+}) and tetrakis (4-carboxyphenyl) porphyrin (TCPP) are prepared via a one-pot reaction. By chelation with the porphyrin structure of TCPP, such Hf-TCPP-PEG NCPs could be easily labeled with $^{99m}Tc^{4+}$, an imaging radioisotope widely used for single-photon emission computed tomography (SPECT) in a clinical environment. Interestingly, Hf, as a high-*Z* element in such ^{99m}Tc-Hf-TCPP-PEG NCPs, could endow nontherapeutic ^{99m}Tc with the therapeutic function of killing cancer cells, likely owing to the interaction of Hf with γ rays emitted from ^{99m}Tc to produce charged particles for radiosensitization. With efficient tumor retention, as revealed by SPECT imaging, our ^{99m}Tc-Hf-TCPP-PEG NCPs offer exceptional therapeutic results in eliminating tumors with moderate doses of ^{99m}Tc after either local or systemic administration. Importantly, those biodegradable NCPs could be rapidly excreted without much long-term body retention. Our work, showing the success of applying NCPs for radioisotope therapy (RIT), presents a potential concept for the realization of highly effective cancer treatment with ^{99m}Tc, a short-half-life (6.0 h) diagnostic radioisotope, which is promising for cancer RIT with enhanced efficacy and reduced side effects.**

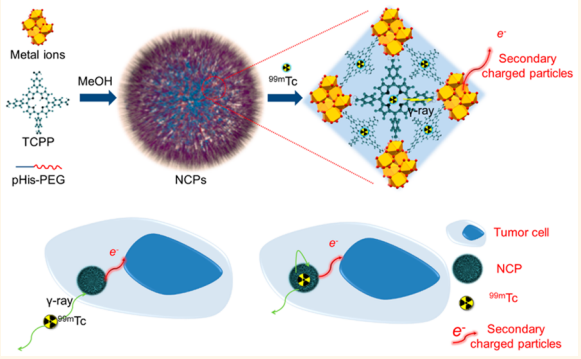

KEYWORDS: *nanoscale coordination polymers, technetium-99, radiosensitization, SPECT imaging, radioisotope therapy*

Radioisotope therapy (RIT) *via* the use of therapeutic radioisotopes (*e.g.*, ^{131}I, ^{125}I, ^{188}Re, ^{177}Lu, etc.),[1−5] most of which are β emitters, implanted or administrated into the tumor or placed nearby the tumor to destruct solid tumors is an widely applied cancer treatment strategy in the clinic.[6,7] However, while local implantation of radioisotopes has no systemic effect on the treatment of metastatic tumors,[8,9] those β-emitting radioisotopes with half-lives of several days, if applied by systemic administration, could result in severe long-lasting damage to normal tissues.[10,11] ^{99m}Tc, as a metastable nuclear isomer of ^{99}Tc, is one of the most widely used radioisotopes in diagnostic imaging, particularly for single-photon emission computed tomography (SPECT).[12−14] With a short half-life of 6.0 h, ^{99m}Tc as a γ emitter is known to be a rather safe radioisotope.[15−17] While it is extensively used as an imaging radioisotope, the use of ^{99m}Tc for RIT has not yet been possible due to the fact that it only emits γ rays that have

Received: March 30, 2018
Accepted: July 13, 2018
Published: July 26, 2018

DOI: 10.1021/acsnano.8b02400
ACS Nano 2018, 12, 7519−7528

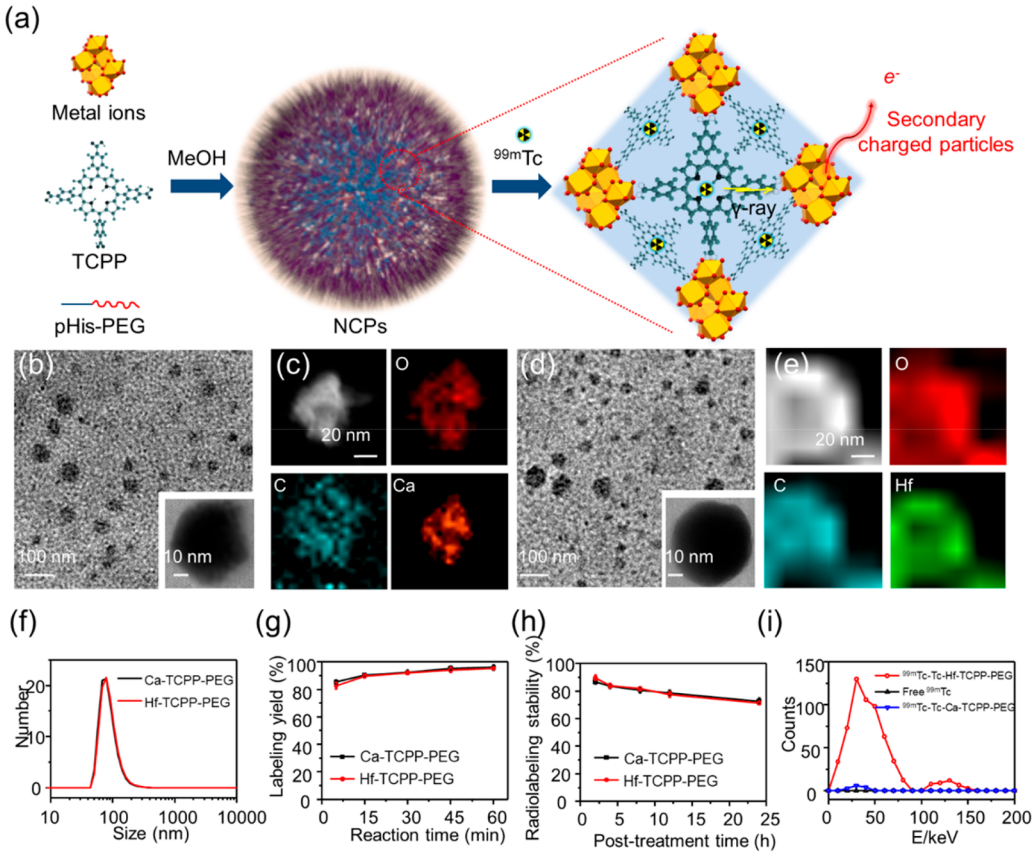

Figure 1. Synthesis and characterization of NCPs. (a) The scheme to illustrate the synthesis, structure, and radiolabeling of Hf-TCPP-PEG NCPs as well as the mechanism of radiosensitization by Hf to generate secondary charged particles after absorbing γ rays emitted from ^{99m}Tc. (b, d) TEM image of the as-synthesized (b) Ca-TCPP-PEG NCPs and (d) Hf-TCPP-PEG NCPs. (c, e) HAADF-STEM element mapping of (c) Ca-TCPP-PEG NCPs and (e) Hf-TCPP-PEG NCPs. (f) The DLS-measured hydrodynamic diameters of Ca-TCPP-PEG and Hf-TCPP-PEG NCPs. (g) The ^{99m}Tc radiolabeling yields for Ca-TCPP-PEG and Hf-TCPP-PEG NCPs achieved by different periods of reaction time. (h) Radiolabeling stability of ^{99m}Tc-Ca-TCPP-PEG and ^{99m}Tc-Hf-TCPP-PEG NCPs in serum. (i) The liquid scintillation spectrum of free ^{99m}Tc, ^{99m}Tc-Ca-NCPs, and ^{99m}Tc-Hf-NCPs to measure generated secondary charged particles (electrons).

little absorption by soft tissues (*e.g.*, tumors) and, thus, much lower damage to cancer cells compared to β particles.[18−21]

Nanoscale coordination polymers (NCPs) are a type of porous nanomaterial formed by coordination interactions between metal cations and multidentate organic ligands.[22,23] Due to a wide selection of metal ions and organic ligands, NCPs can be given judiciously tunable physicochemical properties and have the potential to be used in biomedicine.[24,25] Many research groups, including ours, have reported the application of various types of NCPs as carrier-free nanomedicine platforms for chemotherapy, photodynamic therapy, photothermal therapy, and radiation therapy of cancers.[26−32] One of the key advantages for NCPs compared with typical inorganic nanoparticles is their inherent biodegradability owing to the weak coordination interactions between metal ions and organic linkers.[33,34] However, the application of NCPs for the tumor-targeted delivery of RIT has not been reported to our best knowledge.

In this work, via the self-assembling of metal ions (calcium or hafnium ions) (Ca^{2+} or Hf^{4+}), tetrakis (4-carboxyphenyl) porphyrin (TCPP) as bridging ligands,[35,36] and polyhistidine-polyethylene glycol (pHis-PEG) copolymer as the stabilizing agent, PEGylated NCPs are fabricated by a one-pot reaction method. The obtained Hf-TCPP-PEG and Ca-TCPP-PEG NCPs with similar physicochemical properties can both be easily labeled with an imaging radioisotope ^{99m}Tc (half-life of 6.0 h) by employing TCPP as the chelating agent. Interestingly, different from free ^{99m}Tc and ^{99m}Tc-Ca-TCPP-PEG NCPs, which exert little radiation damage to tumor cells, Hf^{4+}, as a high-Z number within ^{99m}Tc-Hf-TCPP-PEG NCPs, could act as a radiosensitizer to enhance the RIT efficacy of ^{99m}Tc by absorbing γ rays and emitting charged particles.[37−39] At the *in vivo* level, it is discovered by SPECT imaging that ^{99m}Tc-Hf-TCPP-PEG NCPs would show prolonged tumor retention after local intratumoral injection as well as passive tumor homing after intravenous injection. As a result, excellent RIT therapeutic effects have been achieved by ^{99m}Tc-Hf-TCPP-PEG NCPs, which are able to greatly delay tumor growth by single injection or completely eliminate tumors by multiple repeated treatments. Owing to the high safety of ^{99m}Tc with a short half-life as well as the biodegradability of such NCPs, no appreciable systemic toxicity is observed for mice after RIT with ^{99m}Tc-Hf-TCPP-PEG NCPs. Our work thus proposes a potential strategy by which to endow a diagnostic radioisotope with the therapeutic function by using NCPs as the multifunctional carrier for RIT with high efficacy and low side effects.

RESULTS AND DISCUSSION

Hf-TCPP-PEG NCPs and Ca-TCPP-PEG NCPs were synthesized via a one-pot method following our recently

DOI: 10.1021/acsnano.8b02400
ACS Nano 2018, 12, 7519−7528

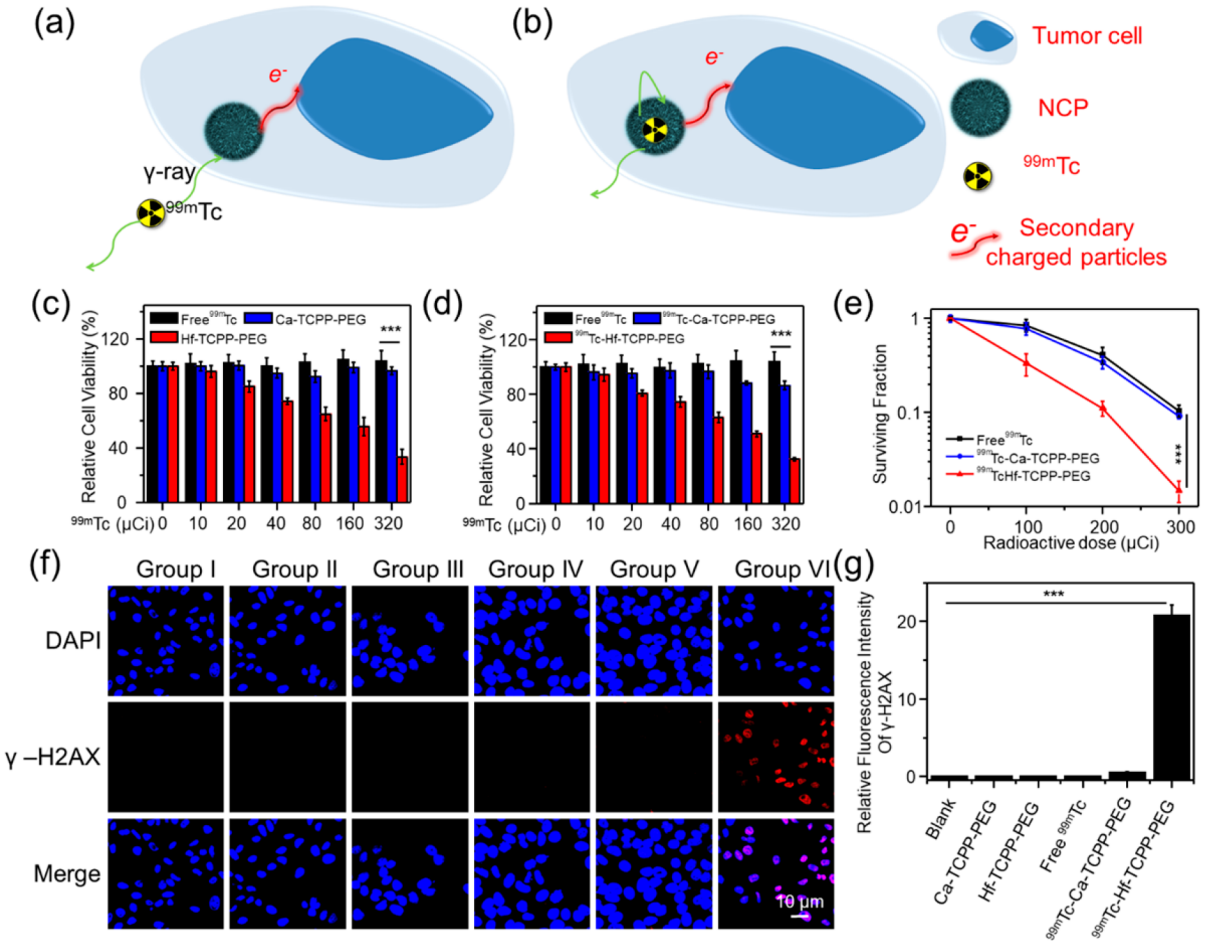

Figure 2. ***In vitro*** **RIT with ^{99m}Tc-Hf-TCPP-PEG NCPs. (a, b) The schemes showing the proposed mechanisms of Hf-sensitized RIT. (a) The ability of preinternalized Hf-containing NCPs within cells to interact with γ rays emitted from ^{99m}Tc for radiosensitization. (b) The "'self-sensitization"' effect by ^{99m}Tc-Hf-TCPP-PEG NCPs of destructing tumor cells. (c) Relative viabilities of 4T1 cells pretreated with Ca-TCPP-PEG or Hf-TCPP-PEG NCPs after incubation with free ^{99m}Tc for 24 h. The RIT effect of free ^{99m}Tc could be enhanced by Hf-TCPP-PEG NCPs. (d) Relative viabilities of 4T1 cells incubated with free ^{99m}Tc, ^{99m}Tc-Ca-TCPP-PEG, and ^{99m}Tc-Hf-TCPP-PEG NCPs with different concentrations for 24 h. ^{99m}Tc-Hf-TCPP-PEG NCPs showed a much-stronger RIT effect compared with free ^{99m}Tc and ^{99m}Tc-Ca-TCPP-PEG NCPs at the same doses. (e) Surviving fractions of 4T1 cells treated with NCPs with free ^{99m}Tc at different dosages (0, 100, 200, 300 μCi) by the colongenic assay. (f) Confocal fluorescence images of γ-H2AX-stained 4T1 cells after various treatments for 24 h. Blue, DAPI; red, γ-H2AX. Groups I, II, III, IV, V, and VI stand for saline, Ca-TCPP-PEG, Hf-TCPP-PEG, free ^{99m}Tc, ^{99m}Tc-Ca-TCPP-PEG, and ^{99m}Tc-Hf-CTPP-PEG, respectively. (g) Relative fluorescence intensities of γ-H2AX-stained 4T1 cells in panel f. *P* values in panels d and e were calculated by Tukey's post-hoc test; triple asterisks indicate $p < 0.001$, double asterisks indicate $p < 0.01$, and single asterisks indicate $p < 0.05$.**

reported method[28] by simply mixing metal ions (Hf^{4+} or Ca^{2+}), TCPP ligands, and pHis-PEG in methanol in room temperature (Figure 1a). In this process, TCPP molecules with four carboxyl groups could form coordination bonds with H^{f4+} or Ca^{2+} ions. Moreover, pHis-PEG was used so that its pHis domain could bind with metal ions, while its PEG domain could offer the obtained NCPs great water solubility and physiological stability. The as-made Hf-TCPP-PEG and Ca-TCPP-PEG NCPs exhibited relatively uniform sizes and similar morphology with transmission electronic microscopy (TEM) (Figure 1b,d). As shown by elemental mapping based on energy-dispersive X-ray (EDX) spectroscopy (Figure 1c,e), Hf^{4+} and Ca^{2+} ions were uniformly dispersed within the respective NCPs. The average hydrodynamic sizes of both NCPs were determined by dynamic light scattering (DLS) to be about 70 nm (Figure 1f). Moreover, both Hf-TCPP-PEG and Ca-TCPP-PEG NCPs showed similar UV−vis absorbance spectra, in which the characteristic absorbance peaks from TCPP could be clearly observed (Figure S1). Those results collectively evidenced the successful formation of NCPs by our one-pot reaction. Owing to the pH responsive charge conversion ability of poly-histidine (pK_a at 6.0), the size of such pHis-PEG modified NCPs showed stable sizes under pH 7.4 but rapidly enlarged sizes under slightly acidic pH (*e.g.*, 5.5), owing to the dissociation of the compact NCP structure after protonation of histidine (Figure S2).

TCPP with the porphyrin structure is able to form chelating complexes with different types of metal ions.[40] We thus speculated that our TCPP-containing NCPs may be labeled with $^{99m}Tc^{4+}$ upon simple mixing. For the radiolabeling experiment, sodium pertechnetate ($Na^{99m}TcO_4$, 1 mCi) was first reduced by sodium borohydride ($NaBH_4$, 0.5 mg/mL) into $^{99m}Tc^{4+}$ and then mixed with Hf-TCPP-PEG or Ca-TCPP-PEG NCPs (2 mg/mL) for radiolabeling by 60 min of incubation. Due to the coordination between TCPP and $^{99m}Tc^{4+}$, NCPs were successfully labeled with ^{99m}Tc. After

DOI: 10.1021/acsnano.8b02400
ACS Nano 2018, 12, 7519−7528

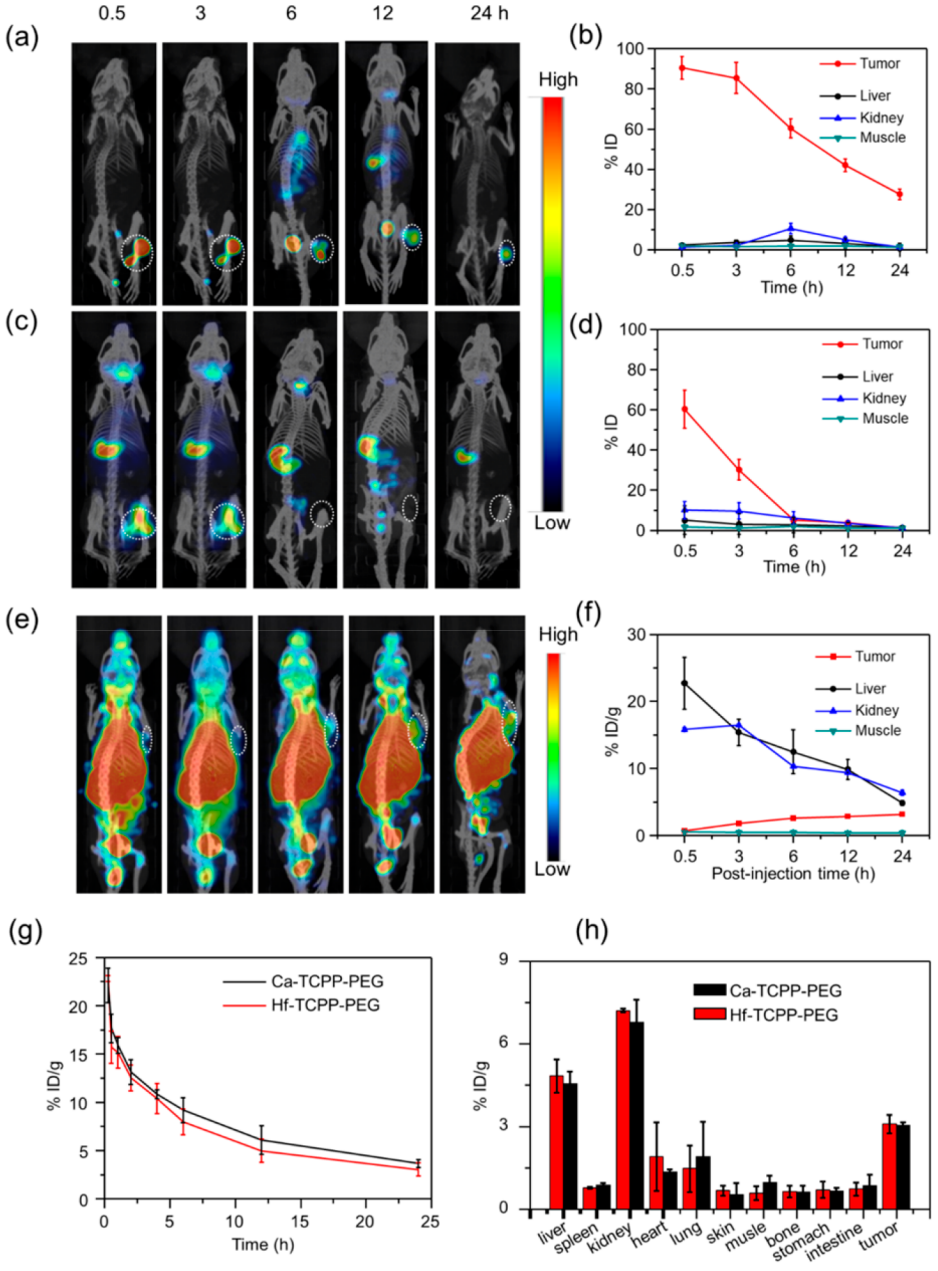

Figure 3. *In vivo* behaviors of NCPs. (a, c) *In vivo* SPECT images of 4T1 tumor-bearing mice after intratumoral local injection with (a) ^{99m}Tc-Hf-TCPP-PEG NCPs or (c) free ^{99m}Tc. (b, d) Quantification of SPECT signals in the tumor, liver, kidney, and muscle tissue for mice at different time points after intratumoral injection with (b) ^{99m}Tc-Hf-TCPP-PEG NCPs or (d) free ^{99m}Tc. (e) *In vivo* SPECT images of 4T1 tumor-bearing mice after intravenous injection with ^{99m}Tc-Hf-TCPP-PEG NCPs. (f) Quantification of SPECT signals in the liver, kidney, tumor, and muscle of 4T1 tumor bearing mice for mice at different time points after intravenous injection with ^{99m}Tc-Hf-TCPP-PEG NCPs. Tumors in panels a, c, and e are highlighted by dashed white circles. (g) The blood circulation profiles of ^{99m}Tc-Ca-TCPP-PEG and ^{99m}Tc-Hf-TCPP-PEG NCPs in mice after intravenous injection. (h) Biodistribution profiles of ^{99m}Tc-Ca-TCPP-PEG and ^{99m}Tc-Hf-TCPP-PEG NCPs measured at 24 h after intravenous injection. Note that all radioactivity signals presented in SPECT imaging and γ counting data have been corrected by the decay half-life of ^{99m}Tc.

purification, the radiolabeling yields were determined to be as high as 95.9 ± 1.8% and 95.3 ± 0.9% for Ca-TCPP-PEG and Hf-TCPP-PEG, respectively (Figures 1g and S3). Little detachment of ^{99m}Tc from ^{99m}Tc-labeled NCPs was observed after incubation in serum at 37 °C for 24 h, suggesting the high radiolabeling stability of ^{99m}Tc-labeled NCPs due to the strong coordination between $^{99m}Tc^{4+}$ and TCPP (Figure 1h).

Compared with soft tissues, nanoparticles containing high-*Z* elements have stronger photoelectric effects. Therefore, high-*Z* elements, upon interaction with X-rays or γ rays, are able to generate secondary charged particles that have relative higher energy deposition in tumor cells, thus enhancing the efficacy of radiotherapy.[41] Because ^{99m}Tc is a pure γ emitter, we thus wondered whether high-Z element like hafnium (Hf) could act as a radiosensitizer to offer ^{99m}Tc the ability to kill tumor cells. To verify the potential radiosensitization ability and understand its mechanism, we used liquid scintillation spectroscopy (Tri-Carb 2910TR Liquid Scintillation Analyzer, PerkinElmer) to measure the emission of charged secondary particles (*e.g.*, β particles) from various formulations of ^{99m}Tc (Figure 1i). As

DOI: 10.1021/acsnano.8b02400
ACS Nano 2018, 12, 7519−7528

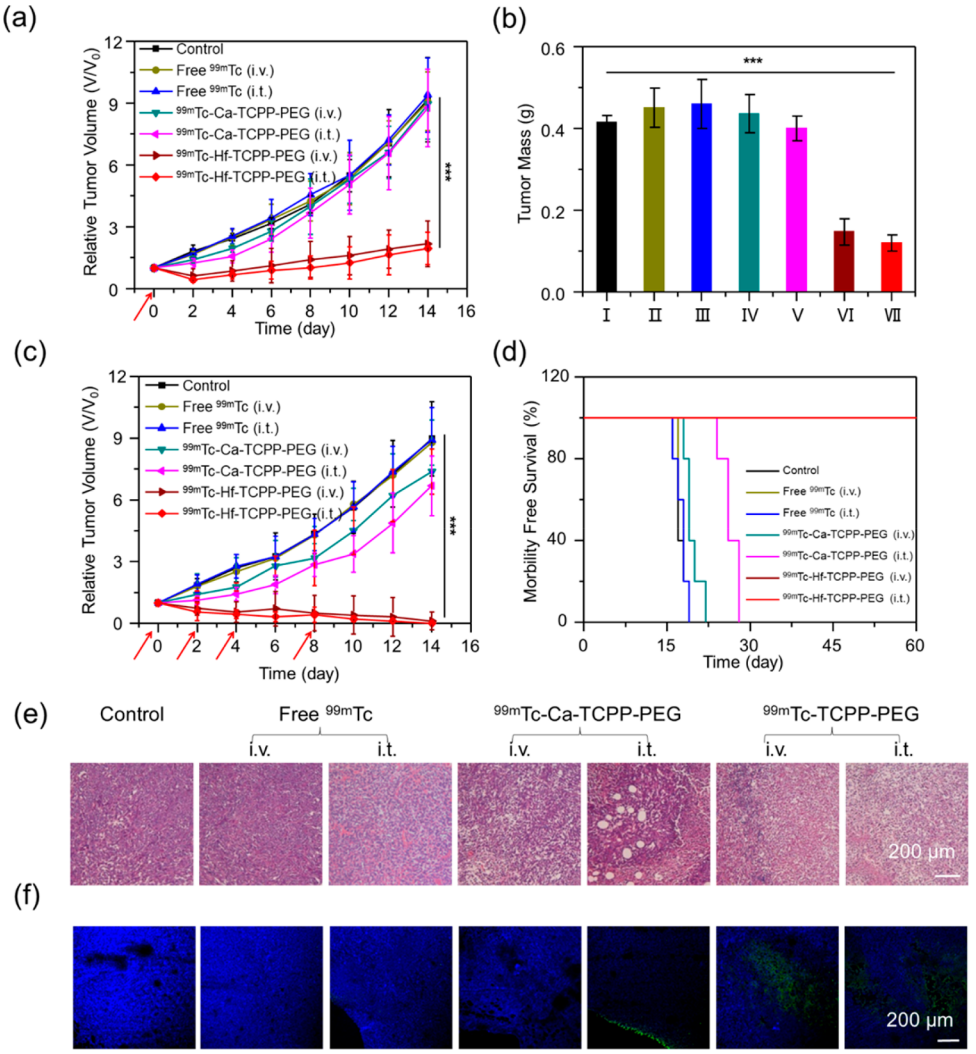

Figure 4. ***In vivo*** **RIT for cancer treatment. (a) Tumor growth curves of mice after single-dose treatment as indicated. (free ^{99m}Tc (300 μCi, intravenous), free ^{99m}Tc (75 μCi, intratumoral), ^{99m}Tc-Ca-TCPP-PEG NCPs (^{99m}Tc: 300 μCi; Ca^{2+}: 20 mg kg^{-1}; intratumoral), ^{99m}Tc-Ca-TCPP-PEG NCPs (^{99m}Tc: 75 μCi; Ca^{2+}: 2.5 mg kg^{-1}; intratumoral), ^{99m}Tc-Hf-TCPP-PEG NCPs (^{99m}Tc: 300 μCi; Hf^{4+}: 20 mg kg^{-1}; intravenous), and ^{99m}Tc-Hf-TCPP-PEG NCPs (^{99m}Tc: 75 μCi; Hf^{4+}: 2.5 mg kg^{-1}; intratumoral). (b) Average tumor weights from different groups of mice collected at the 14th day after the initiation of treatments. (c) Tumor growth curves of mice after multidose treatments as indicated (the doses were the same as those indicated in panel a. (d) Morbidity-free survival curves for different groups of mice in panel c. Note that the last two groups, ^{99m}Tc-Hf-TCPP-PEG treatment by intravenous or intratumoral injection, showed overlapped survival curves (100% survival over 60 days). (e, f) Micrographs of (e) H&E-stained and (f) immunofluorescence TUNEL-stained tumor slices collected from different groups of mice at 24 h after the first dose. *P* values in panels d and e were calculated by Tukey's post-hoc test; triple asterisks indicate $p < 0.001$, double asterisks indicate $p < 0.01$, and single asterisks indicate $p < 0.05$).**

expected, free ^{99m}Tc (1 mCi), as a pure γ emitter, showed no detectable signals in the scintillation spectrum. While a small peak was observed in the scintillation spectrum of ^{99m}Tc-Ca-TCPP-PEG, ^{99m}Tc-Hf-TCPP-PEG NCPs showed a strong peak at 30 keV, indicating the effective production of charged secondary particles from such Hf-based NCPs with ^{99m}Tc labeling. Our results indicate that γ rays emitted from ^{99m}Tc would be able to interact with high-Z elements to trigger the production of charged secondary particles (*e.g.*, auger electrons). Compared to Ca, Hf with a much higher atomic number would thus have a much stronger radiosensitization effect.

Next, we conducted *in vitro* experiments to verify the possibility of using diagnostic radioisotope ^{99m}Tc for RIT via the mechanism of radiosensitization by Hf-based NCPs (Figure 2a,b). First, 4T1 murine breast cancer cells were pretreated with "cold" NCPs (Ca-TCPP-PEG or Hf-TCPP-PEG) without radiolabeling at the same concentration (50 μg/mL). Those cells were washed to remove excess NCPs after 24 h of incubation and then exposed to different doses of free ^{99m}Tc (0, 10, 20, 40, 80, 160, and 320 μCi/mL) for another 24 h before the standard cell viability assay. Compared with cells pretreated with Ca-TCPP-PEG NCPs, cells pretreated with Hf-TCPP-PEG NCPs showed significantly enhanced ^{99m}Tc-induced cell damages despite there being no appreciable cytotoxicity of NCPs toward those cells (Figure 2c). Notably, direct exposure of cells to free ^{99m}Tc without pretreatment with NCPs showed no appreciable effect to the cell viability, suggesting the little radiotherapeutic toxicity of ^{99m}Tc. Therefore, our results indicated that Hf as a high-Z element in Hf-TCPP-PEG NCPs should have the sensitization capability to convert nontherapeutic radioisotopes such as

DOI: 10.1021/acsnano.8b02400
ACS Nano 2018, 12, 7519−7528

^{99m}Tc into a therapeutic one by absorbing γ-ray emission from ^{99m}Tc to generate charged secondary particles that were toxic to tumor cells.

The *in vitro* RIT therapeutic effects of ^{99m}Tc-labeled NCPs were then evaluated. In this ^{99m}Tc-Hf-TCPP-PEG system, the labeled ^{99m}Tc could act as a radio-emitter, while Hf within NCPs could serve as a radiosensitizer to adsorb γ-ray emission and produce secondary charged particles to destruct cancer cells. 4T1 cells were incubated with free ^{99m}Tc, ^{99m}Tc-Ca-TCPP-PEG or ^{99m}Tc-Hf-TCPP-PEG NCPs at different concentrations for 24 h before the cell viability assay. With the help of the radiosensitization effect of Hf, cells treated with ^{99m}Tc-Hf-TCPP-PEG NCPs showed significantly reduced viabilities compared with those treated with free ^{99m}Tc or ^{99m}Tc-Ca-TCPP-PEG NCPs at the same radioactivity doses (Figure 2d). Similar results were also found for another tumor cell line, CT26 colon cancer cells (Figure S4). Moreover, we found that ^{99m}Tc-Hf-TCPP-PEG NCPs showed significantly increased cell internalization efficiency compared to free ^{99m}Tc, another reason attributed to the high *in vitro* RIT efficacy of such ^{99m}Tc-Hf-TCPP-PEG NCPs (Figure S5).

To further confirm the RIT-sensitization capacity of Hf-TCPP-PEG NCPs, the clonogenic assay was also carried out. Consistent with cell viability data, cells incubated with ^{99m}Tc-Hf-TCPP-PEG NCPs showed lower percentages of viable cell colonies compared with those incubated with ^{99m}Tc-Ca-TCPP-PEG NCPs or free ^{99m}Tc. The sensitization enhancement ratio (SER), which was used to evaluate the effect of a radiosensitizer,[5] was calculated to be 1.39 for Hf-TCPP-PEG NCPs (Figure 2e). Furthermore, immunofluorescence staining of γ-H2AX, a well-known marker of double-strand DNA breaks, was applied to evaluate DNA damages in cancer cells induced by RIT. While unlabeled NCPs, free ^{99m}Tc, or ^{99m}Tc-Ca-TCPP-PEG induced no or little DNA damages to cells, obviously enhanced DNA damage was detected for the ^{99m}Tc-Hf-TCPP-PEG NCPs treated group at 12 and 24 h (Figures 2f,g and S6). Therefore, our results strongly evidenced the remarkable RIT enhancement effect of those Hf-containing NCPs with ^{99m}Tc labeling.

^{99m}Tc was widely used for disease diagnosis in the clinic. Utilizing the radioactivity of ^{99m}Tc, we could quantitatively track the *in vivo* behaviors of those NCPs. We first studied the tumor retention of ^{99m}Tc-NCPs after intratumoral (intratumoral) local injection. Tumor bearing mice were intratumoral injected with free ^{99m}Tc or ^{99m}Tc-Hf-TCPP-PEG NCPs (Hf^{4+}: 2.5 mg kg $^{-1}$; ^{99m}Tc: 200 μCi) and then scanned under SPECT imaging. It was found that free ^{99m}Tc, which showed rapid diffusion from the injection site to other normal organs and little tumor retention after 6 h post-injection. In marked contrast, ^{99m}Tc-Hf-TCPP-PEG NCPs exhibited greatly prolonged tumor retention and little accumulation in normal organs after local injection into tumors (Figure 3a−d). *Ex vivo* biodistribution data showed that the use of intratumoral injection could significantly reduce the unwanted distribution of radioactivities in other normal organs (Figure S7), which is promising for applications in RIT cancer treatment.

Thereafter, we further evaluated the tumor homing ability of those NCPs after intravenous injection. Mice were intravenously injected with ^{99m}Tc-Ca-TCPP-PEG or ^{99m}Tc-Hf-TCPP-PEG NCPs (Ca^{2+} or Hf^{4+}: 20 mg kg $^{-1}$; ^{99m}Tc: 1 mCi) and then scanned under SPECT imaging (Figures 3e and S8). Upon intravenous injection of the two types of NCPs, SPECT signals showed up in the tumors, evidencing time-dependent tumor homing of NCPs (Figures 3f and S9). The accuracy of SPECT imaging was validated by ex vivo biodistribution data (Figure 3h), which correlated well with the region-of-interest (ROI) data from the SPECT images. Moreover, the blood-circulation behaviors of ^{99m}Tc-Ca-TCPP-PEG or ^{99m}Tc-Hf-TCPP-PEG NCPs after intravenous injection were found to be quite similar, both showing prolonged blood half-lives (^{99m}Tc-Hf-TCPP-PEG NCPs: $t_{1/2\alpha}$ = 0.72 h, $t_{1/2\beta}$ = 6.32 h; ^{99m}Tc-Ca-TCPP-PEG: $t_{1/2\alpha}$ = 0.77 h, $t_{1/2\beta}$ = 6.66 h; Figure 3g). Therefore, as the result of the enhanced permeability and retention (EPR) effect, both types of NCPs exhibited similar *in vivo* behaviors and tumor passive uptake.

Next, the *in vivo* therapeutic efficacy of ^{99m}Tc-Hf-TCPP-PEG NCPs was evaluated after either intravenous systemic administration or intratumoral local injection of different formulations of ^{99m}Tc into mice bearing 4T1 tumors. In this experiment, we randomly divided mice into 7 groups (n = 5 per group) for the following treatments: saline, free ^{99m}Tc (300 μCi, intravenous), free ^{99m}Tc (75 μCi, intratumoral), ^{99m}Tc-Ca-TCPP-PEG NCPs (^{99m}Tc: 300 μCi; Ca^{2+}: 20 mg kg^{-1}; intravenous), ^{99m}Tc-Ca-TCPP-PEG NCPs (^{99m}Tc: 75 μCi; Ca^{2+}: 2.5 mg kg^{-1}; intratumoral), ^{99m}Tc-Hf-TCPP-PEG NCPs (^{99m}Tc: 300 μCi; Hf^{4+}: 20 mg kg^{-1}; intravenous), and ^{99m}Tc-Hf-TCPP-PEG NCPs (^{99m}Tc: 75 μCi; Hf^{4+}: 2.5 mg kg^{-1}; intratumoral) for the single-dose treatment. The tumor sizes were monitored afterward for 14 days (Figure 4a) before the tumors were collected and weighed (Figure 4b). Treatment with free ^{99m}Tc or ^{99m}Tc-Ca-TCPP-PEG NCPs, regardless of the administration route, exhibited no obvious effect to the tumor growth. In contrast, ^{99m}Tc-Hf-TCPP-PEG NCPs treatment by either intratumoral or intravenous injection resulted in significantly suppressed tumor growth, demonstrating the effective radiotherapeutic effect of such ^{99m}Tc-labeled, Hf-containing NCPs owing to the "self-sensitization" mechanism.

To further improve the therapeutic efficacy, we then conducted another around of treatment experiments by giving mice repeated doses. A total of seven groups of mice bearing 4T1 tumors were administrated with saline, free ^{99m}Tc (intravenous), free ^{99m}Tc (intratumoral), ^{99m}Tc-Ca-TCPP-PEG NCPs (intravenous), ^{99m}Tc-Ca-TCPP-PEG NCPs (intratumoral), ^{99m}Tc-Hf-TCPP-PEG NCPs (intravenous), and ^{99m}Tc-Hf-TCPP-PEG NCPs (intratumoral) at different time points (0, 2, 4, and 8 days post-injection) for the multidose treatment (Figure 4c). The radioactivity doses were 300 and 75 μCi for intravenous and intratumoral injections, respectively, at each dose. Compared to free ^{99m}Tc, which showed no appreciable tumor growth inhibition effect even after four repeated doses, ^{99m}Tc-Ca-TCPP-PEG NCPs with multidose treatment could slightly delay the tumor growth, likely owing to the weak interaction between ^{99m}Tc and Ca^{2+} ions (Figure 1i) Notably, tumors on all the five mice disappeared after treatment with ^{99m}Tc-Hf-TCPP NCPs by either intravenous. or intratumoral administration (Figure 4c). Those mice became tumor-free and survived for over two months, which is in marked contrast to the short life spans of mice in other control groups: 16−20 days for untreated and free-^{99m}Tc-treated mice and 18−22 days for ^{99m}-Tc-Ca-TCPP-PEG-treated mice (Figure 4d). Moreover, as evidenced by hematoxylin and eosin (H&E) and terminal deoxynucleotidyl transferase dUTP nick-end labeling (TUNEL) staining of tumor slices collected 1 day after the first dosing, the most-

DOI: 10.1021/acsnano.8b02400
ACS Nano 2018, 12, 7519−7528

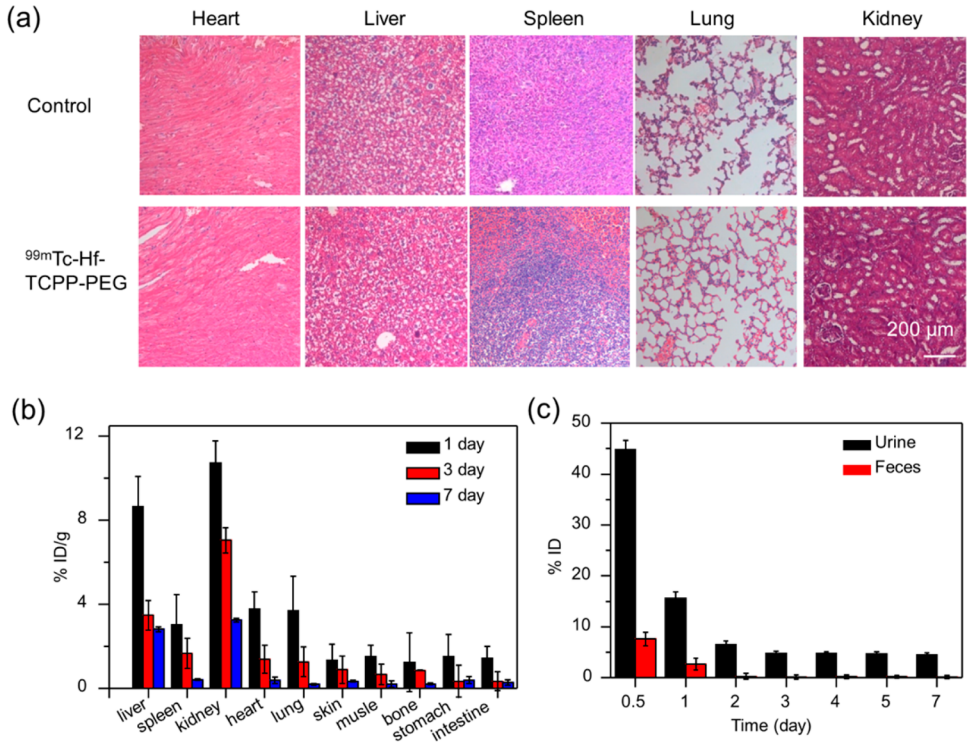

Figure 5. ***In vivo*** **toxicity and excretion studies. (a) Representative micrographs of H&E-stained major organ slices from healthy untreated mice and mice survived after RIT with four repeated doses of ^{99m}Tc-Hf-TCPP-PEG (intravenous injection). (b) Time-dependent biodistribution of Hf in mice after intravenous injection of Hf-TCPP-PEG NCPs. (c) Hf levels in urine and feces samples collected from mice at different time points after intravenous injection of Hf-TCPP-PEG.**

significant tumor cell damage and apoptosis were observed for tumors on mice after RIT with ^{99m}Tc-Hf-TCPP-PEG NCPs (Figure 4e,f).

As far as the potential side effects are concerned, it was found that mice that were injected with ^{99m}Tc-NCPs showed no appreciable body weight drop and no abnormal behaviors after treatment (Figure S10). Histological examination by H&E-stained organ slices uncovered no notable sign of organ damage for mice that survived for over 60 days after multiple doses of NCPs-enhanced RIT (Figure 5a). To further study the excretion kinetics of those NCPs, healthy Balb/c mice with intravenous injections of Hf-TCPP-PEG NCPs were sacrificed at different time points: 1, 3, and 7 days post-injection. As determined by inductively coupled plasma atomic emission spectrometry (ICP-AES) (Figure 5b), the Hf contents in the liver and spleen of those mice were measured to be ~8.7 and ~3.0% of injected dose per gram of tissue (%ID/g) at 1 day post-injection and decreased to rather low levels later on. Notably, high Hf^{4+} levels were found in kidneys, indicating that NCPs, after degradation into small molecules and ions, might be quickly excreted via renal excretion through kidneys. Next, we measured Hf^{4+} concentrations in excreta from NCP-injected mice by ICP-AES (Figure 5c). Within the first 12 h, ~45.5% and ~7.6% of injected Hf were excreted via urine and feces, respectively. High levels of Hf^{4+} were detected, mainly in the urine of mice in the following days, another strong indication of the biodegradation of those NCPs. Moreover, we observed similar *in vivo* excretion kinetics for Ca-TCPP-PEG NCPs (Figure S11). To further study the potential *in vivo* toxicity of ^{99m}Tc-Hf-TCPP-PEG NCPs, a serum biochemistry assay and a complete blood panel test were conducted for mice that were intravenously injected with ^{99m}Tc-Hf-TCPP-PEG NCPs on days 1, 7, and 14. Compared to healthy control mice, no significant abnormality was observed for mice treated with ^{99m}Tc-labeled NCPs (Figure S12). Therefore, our results evidenced that the two types of NCPs within the mouse body could be degraded and then effectively cleared out in a relatively rapid manner without causing long-term toxicity to the treated animals.

CONCLUSIONS

In summary, PEGylated NCPs containing Hf as the high-*Z* element and TCPP as the chelating molecule are fabricated by a one-pot method in this work. The obtained Hf-TCPP-PEG NCPs can be labeled with ^{99m}Tc, a commonly used diagnostic radioisotope, with a high radiolabeling efficiency (~95%) and great labeling stability depending on the coordination between TCPP and $^{99m}Tc^{4+}$. Interestingly, owing to the strong interactions between γ rays emitted from ^{99m}Tc and a Hf element within such NCPs to generate secondary charged particles that have stronger energy deposition in cells, anchoring ^{99m}Tc into Hf-containing NCPs could offer this nontherapeutic radioisotope a therapeutic function of killing tumor cells. We further utilize the γ emission of ^{99m}Tc to track the *in vivo* behaviors of ^{99m}Tc-labeled NCPs by SPECT imaging, which uncovers prolonged tumor retention of radioactivity after local administration, as well as the efficient passive tumor homing of those NCPs after intravenous injection by the EPR effect. As the results showed, improved *in vivo* therapeutic outcomes were achieved by RIT with ^{99m}Tc-Hf-TCPP-PEG NCPs. Moreover, with inherent biodegradability, those NCPs exhibit efficient clearance from the mouse body with little long-term retention, which is promising for future possible clinical translation. Our work not only presents

DOI: 10.1021/acsnano.8b02400
ACS Nano 2018, 12, 7519−7528

the great potential of the application of NCPs as an intelligent type of tumor-targeting RIT platform but also demonstrates the possibility of applying a diagnostic radioisotope, ^{99m}Tc with a short half-life (6.0 h) and pure γ emission, for the effective RIT treatment of tumors. Such a strategy is particularly meaningful to achieve RIT with high safety and greatly reduced side effects compared to conventional RIT using β-emitting radioisotopes with half-lives of many days (*e.g.*, ^{177}Lu, ^{186}Re, ^{32}P, etc.) or even months (^{125}I).

MATERIALS AND METHODS

Materials and Characterization. Tetrakis (4-carboxyphenyl) porphyrin (TCPP) was bought from TCI, Shanghai, China. Hafnium(IV) tetrachloride ($HfCl_4$) was bought from Alfa Aesar (China) Chemicals Co. Ltd. Calcium chloride ($CaCl_2$) was bought from Shanghai Lingfeng Chemical Reagent Co. Ltd. Poly-L-histidine (pHis) was bought from GL Biochem (Shanghai) Ltd. PEG polymers were bought from PegBio, Suzhou, China. Radioisotope sodium pertechnetate (^{99m}Tc) was bought from Shanghai GMS pharmaceutical Co. Ltd. All other chemical reagents were purchased from Sigma-Aldrich and used as received without any purification. An FEI Tecnai F20 transmission electron microscope was used to characterize the morphology of those NCPs. The hydrodynamic diameters and ζ potentials of the NCPs were determined by a Zetasizer Nano-ZS (Malvern Instruments).

Synthesis of Hf-TCPP-PEG and Ca-TCPP-PEG NCPs. The copolymer pHis-PEG was prepared following a literature protocol.[28] To fabricate NCPs, 1 mmol of hafnium tetrachloride ($HfCl_4$) or 2 mmol of calcium chloride ($CaCl_2$) was dissolved in 60 mL of methanol in the presence of 100 μL of triethylamine (TEA). Afterward, 5 mg of pHis-PEG and 2 mmol of TCPP were added dropwise into the previously mentioned solution. After stirring for 12 h at room temperature, methanol was evaporated by rotary evaporation, and the sample was dialyzed against water for another 2 days. The purified NCPs were stored at 4 °C for future use.

^{99m}Tc Radiolabeling and Labeling Stability Assay. First, radioactive sodium pertechnetate ($Na^{99m}TcO_4$) was reduced from $^{99m}Tc^{VII}$ to $^{99m}Tc^{IV}$ by sodium borohydride ($NaBH_4$). A total of 200 μL of Hf-TCPP-PEG or Ca-TCPP-PEG NCPs was mixed with 200 μL of $NaBH_4$ in a 1.5 mL tube, into which 200 μL of $Na^{99m}TcO_4$ was immediately added. The mixed solution was incubated at 37 °C for 60 min with constant shaking. The yielded ^{99m}Tc-Hf-TCPP-PEG NCPs and ^{99m}Tc-Ca-TCPP-PEG NCPs were purified by size-exclusion column using PBS as the mobile phase. The labeling yield was measured by thin-layer chromatography (TLC). To determine the labeling stability, the radiolabeled NCPs were incubated with serum for 24 h at 37 °C. Portions of the mixtures were sampled at different time points (2, 4, 8, 12, and 24 h) and filtered through 100 kDa molecular-weight cut-off (MWCO) filters. The radioactivity remained on the filter was measured by γ counter (PerkinElmer) after discarding the filtrate. To measure the liquid scintillation spectrum, 100 μL of free ^{99m}Tc, ^{99m}Tc-Ca-NCPs, or ^{99m}Tc-Hf-NCPs was mixed with 2 mL of PE scintillation liquid (PerkinElmer) and put into the detector of the liquid scintillation analyzer (PerkinElmer, Tri-Carb 2910TR).

***In Vitro* Cell Experiments.** Murine breast cancer 4T1 cells were cultured under the standard condition. To investigate the "self-sensitizing" mechanism of Hf-TCPP-PEG NCPs, we pre-incubated cells with "cold" Hf-TCPP-PEG (30 μg/mL) or Ca-TCPP-PEG NCPs (50 μg/mL) without radiolabeling for 24 h and then re-incubated them with different concentrations of free ^{99m}Tc at 0, 5, 10, 20, 40, 80, and 160 μCi mL^{-1} for 24 h. Relative cell viabilities were determined by 3-(4,5-dimethyl-2-thiazolyl)-2,5-diphenyl-2-H-tetrazolium bromide (MTT) assay. For *in vitro* RIT, cells were treated with free ^{99m}Tc, ^{99m}Tc-Ca-TCPP-PEGm, and ^{99m}Tc-Hf-TCPP-PEG NCPs with different radioactive dosages at 0, 5, 10, 20, 40, 80, and 160 μCi mL^{-1} for 24 h. MTT assay was then conducted to investigate the relative cell viabilities.

For the γ-H2AX immunofluorescence staining, 4T1 cells pre-seeded in six-well plates were incubated with NCPs (30 μg mL^{-1}) or ^{99m}Tc-NCPs for 4 h. After another 12 or 24 h of incubation, cells were stained with γ-H2AX and DAPI per our previous report. The cells were imaged using confocal microscopy (Leica SP5).

For the clonogenic assay, 4T1 cancer cells were seeded into six-well plates at densities of 20, 50, 100, 200, and 500 cells per well. After 24 h, cells were treated with 50 μg mL^{-1} of ^{99m}Tc radiolabeled NCPs at various radiation doses (0, 100, 200, and 300 μCi) for 6 h. Cells were cultured for another 7 days and fixed with anhydrous ethanol and stained with crystal violet. The surviving fraction was equal to the number of surviving colonies divided by the product of the cells seeded and the plating efficiency, all multiplied by 100%.

***In Vivo* Tumor Model.** Balb/c mice were purchased from the Soochow University Laboratory Animal Center and used under the approved protocols. To prepare the tumor model, 4T1 cells (2×10^6) suspended in 25 μL of PBS were subcutaneously injected into the back of each Balb/c mouse.

***In Vivo* SPECT Imaging and Biodistribution Investigation.** Mice bearing 4T1 tumors were intravenously injected with ^{99m}Tc-Hf-TCPP-PEG or ^{99m}Tc-Ca-TCPP-PEG NCPs or intratumorally injected with free ^{99m}Tc or ^{99m}Tc-Hf-TCPP-PEG NCPs for serial SPECT scans using a U-SPECT+/CT imaging system (MILABS) at different time points (0.5, 4, 12, and 24 h) post-injection. After completion of the SPECT imaging at 24 h post-injection, mice were sacrificed to collect their major organs for *ex vivo* biodistribution studies by a γ counter. The biodistribution data were presented as the percent of injected dose per gram of tissue (%ID/g) by mean ± standard deviation.

***In Vivo* Biodistribution and Clearance Study.** For the biodistribution study, healthy Balb/c mice were intravenously injected with 0.2 mL of Hf-TCPP-PEG or Ca-TCPP-PEG NCPs and scarified at different time points (1, 3, and 7 days post-injection, n = 5 mice per group). Another five mice that were not given injections were used to eliminate the effects of original Ca^{2+}/Hf^{4+} in these organs and tissues. The major organs were solubilized in chloroazotic acid and then diluted by deionized water to 10 mL. ICP-AES (Vista Mpx 700-ES) was employed to determine the concentrations of Hf^{4+} or Ca^{2+} in those samples. Mice that were not given injections of NCPs were used to determine the background Ca^{2+}/Hf^{4+} signals in these organs/tissues. To study the excretion of Hf-TCPP-PEG, mice were housed in metabolic cages to collect their urine and feces, which were also digested by chloroazotic acid for ICP-AES measurement.

***In Vivo* Radioisotope Therapy.** For single-dose treatment, mice were randomly divided into 7 groups after the tumors had reached ~50 mm^3 (n = 5 for each group). Mice were intravenously injected with saline, free ^{99m}Tc (300 μCi), ^{99m}Tc-Ca-TCPP-PEG NCPs (^{99m}Tc: 300 μCi; Ca2+: 20 mg kg-1; intravenous), ^{99m}Tc-Ca-TCPP-PEG NCPs (^{99m}Tc: 75 μCi; Ca2+: 2.5 mg kg^{-1}; intratumoral), ^{99m}Tc–Hf-TCPP-PEG NCPs (99 mTc: 300 μCi; Hf^{4+}: 20 mg kg^{-1}; intravenous), and ^{99m}Tc-Hf-TCPP-PEG NCPs (^{99m}Tc: 75 μCi; Hf^{4+}: 2.5 mg kg^{-1}; intratumoral) at day 0. For multidose treatment, mice were randomly divided into 7 groups after the tumors had reached ~50 mm^3 (n = 5 for each group). Mice were intravenously injected with saline, free ^{99m}Tc (300 μCi), ^{99m}Tc-Ca-TCPP-PEG NCPs (^{99m}Tc: 300 μCi; Ca2+: 20 mg kg^{-1}; intravenous), ^{99m}Tc-Ca-TCPP-PEG NCPs (^{99m}Tc: 75 μCi; Ca2+: 2.5 mg kg^{-1}; intratumoral), ^{99m}Tc-Hf-TCPP-PEG NCPs (^{99m}Tc: 300 μCi; Hf4+: 20 mg kg^{-1}; intravenous), and ^{99m}Tc-Hf-TCPP-PEG NCPs (^{99m}Tc: 75 μCi; Hf4+: 2.5 mg kg^{-1}; intratumoral) at different time points (0, 2, 4, and 8 days). The tumor sizes were calculated as volume equal to the squared product of the tumor length and tumor width, all divided by 2. For relative tumor volumes, V_0 was the initial tumor size right prior to the treatment. However, tumors from all 7 treated group were collected 1 day post-treatment for H&E and TUNEL staining and examined with a fluorescence microscope (Olympus).

For blood biochemistry and complete blood analysis, healthy mice (n = 5) were randomly divided into 4 groups and intravenously injected with saline or ^{99m}Tc-Hf-TCPP-PEG NCPs. Blood sample

DOI: 10.1021/acsnano.8b02400
ACS Nano 2018, 12, 7519–7528

were collect from the mice on days 1, 7, and 14 and measured by Wuhan Biological Technology Service Co. Ltd.

ASSOCIATED CONTENT

Supporting Information

The Supporting Information is available free of charge on the ACS Publications website at DOI: 10.1021/acsnano.8b02400.

Figures showing absorption spectra, γ images of TLC plates, relative viabilities, cell uptake, confocal fluorescence images, biodistribution profiles, SPECT images, time-dependent changes of tumor-to-muscle ratios, body weight of mice, and time-dependent biodistribution. (PDF)

AUTHOR INFORMATION

Corresponding Authors

*E-mail: zliu@suda.edu.cn.
*E-mail: kyang@suda.edu.cn.
*E-mail: wusong@szu.edu.cn.

ORCID

Yu Yang: 0000-0002-4518-3299
Kai Yang: 0000-0002-6670-1024
Zhuang Liu: 0000-0002-1629-1039

Notes

The authors declare no competing financial interest.

ACKNOWLEDGMENTS

This work was partially supported by the National Basic Research Programs of China (grant no. 2016YFA0201200), the National Natural Science Foundation of China (grant nos. 51525203, 51761145041, and 81471716), Collaborative Innovation Center of Suzhou Nano Science and Technology, and a Project Funded by the Priority Academic Program Development (PAPD) of Jiangsu Higher Education Institutions.

REFERENCES

(1) Hainfeld, J. F.; Slatkin, D. N.; Smilowitz, H. M. The Use of Gold Nanoparticles to Enhance Radiotherapy in Mice. *Phys. Med. Biol.* **2004**, *49*, N309.

(2) Mills, R. L.; Walter, C. W.; Venkataraman, L.; Pang, K.; Farrell, J. J. A Novel Cancer-Therapy using a Mossbauer-Isotope Compound. *Nature* **1988**, *336*, 787−789.

(3) Kwekkeboom, D. J.; Bakker, W. H.; Kam, B. L.; Teunissen, J. J. M.; Kooij, P. P. M.; Herder, W. W.; Feelders, R. A.; Eijck, C. H. J.; Jong, M.; Srinivasan, A.; Erion, J. L.; Krenning, E. P. Treatment of Patients with Gastro-Entero-Pancreatic (GEP) Tumours with the Novel Radiolabelled Somatostatin Analogue Lu-177-DOTA(0),-Tyr(3) Octreotate. *Eur. J. Nucl. Med. Mol. Imaging* **2003**, *30*, 417−422.

(4) Yi, X.; Yang, K.; Liang, C.; Zhong, X.; Ning, P.; Song, G.; Wang, D.; Ge, C.; Chen, C.; Chai, Z.; Liu, Z. Imaging-Guided Combined Photothermal and Radiotherapy to Treat Subcutaneous and Metastatic Tumors Using Iodine-131-Doped Copper Sulfide Nanoparticles. *Adv. Funct. Mater.* **2015**, *25*, 4689−4699.

(5) Song, G.; Cheng, L.; Chao, Y.; Yang, K.; Liu, Z. Emerging Nanotechnology and Advanced Materials for Cancer Radiation Therapy. *Adv. Mater.* **2017**, *29*, 1700996.

(6) Hammond, A. L. Cancer Radiation-Therapy - Potential for High-Energy Particles. *Science* **1972**, *175*, 1230.

(7) D'Amico, A. V.; Whittington, R.; Malkowicz, S. B.; Schultz, D.; Blank, K.; Broderick, G. A.; Tomaszewski, J. E.; Renshaw, A. A.; Kaplan, I.; Beard, C. J.; Wein, A. Biochemical Outcome after Radical Prostatectomy, External Beam Radiation Therapy, or Interstitial Radiation Therapy for Clinically Localized Prostate Cancer. *Jama-J.e Am. Med. Asso.* **1998**, *280*, 969−974.

(8) Han, K.; Milosevic, M.; Fyles, A.; Pintilie, M.; Viswanathan, A. N. Trends in the Utilization of Brachytherapy in Cervical Cancer in the United States. *Int. J. Radiat. Oncol., Biol., Phys.* **2013**, *87*, 111−119.

(9) Maier-Hein, L.; Vedula, S. S.; Speidel, S.; Navab, N.; Kikinis, R.; Park, A.; Eisenmann, M.; Feussner, H.; Forestier, G.; Giannarou, S.; Hashizume, M.; Katic, D.; Kenngott, H.; Kranzfelder, M.; Malpani, A.; März, K.; Neumuth, T.; Padoy, N.; Pugh, C.; Schoch, N.; Stoyanov, D.; Taylor, R.; Wagner, M.; Hager, G. D.; Jannin, P. Surgical Data Science for Next-Generation Interventions. *Nat. Biomed. Eng.* **2017**, *1*, 691−696.

(10) Thorne, M. C.; Vennart, J. Toxicity of Sr-90, Ra-226 and Pu-239. *Nature* **1976**, *263*, 555−558.

(11) Volkert, W. A.; Goeckeler, W. F.; Ehrhardt, G. J.; Ketring, A. R. Therapeutic Radionuclides - Production and Decay Property Consideration. *J. Nucl. Med.* **1991**, *32*, 174−185.

(12) Robu, S.; Schottelius, M.; Eiber, M.; Maurer, T.; Gschwend, J.; Schwaiger, M.; Wester, H.-J. Preclinical Evaluation and First Patient Application of Tc-99m-PSMA-I&S for SPECT Imaging and Radioguided Surgery in Prostate Cancer. *J. Nucl. Med.* **2017**, *58*, 235−242.

(13) Heinzmann, K.; Carter, L. M.; Lewis, J. S.; Aboagye, E. O. Multiplexed Imaging for Diagnosis and Therapy. *Nat. Biomed. Eng.* **2017**, *1*, 697−713.

(14) Hong, H.; Zhang, Y.; Sun, J.; Cai, W. Molecular Imaging and Therapy of Cancer with Radiolabeled Nanoparticles. *Nano Today* **2009**, *4*, 399−413.

(15) Funk, T.; Sun, M. S.; Hasegawa, B. H. Radiation Dose Estimate in Small Animal SPECT and PET. *Med. Phys.* **2004**, *31*, 2680−2686.

(16) Yun, S. H.; Kwok, S. J. J. Light in Diagnosis, Therapy and Surgery. *Nat. Biomed. Eng.* **2017**, *1*, 0008.

(17) Yu, X.; Gao, D.; Gao, L.; Lai, J.; Zhang, C.; Zhao, Y.; Zhong, L.; Jia, B.; Wang, F.; Chen, X.; Liu, Z. Inhibiting Metastasis and Preventing Tumor Relapse by Triggering Host Immunity with Tumor-Targeted Photodynamic Therapy Using Photosensitizer-Loaded Functional Nanographenes. *ACS Nano* **2017**, *11*, 10147−10158.

(18) Hempelmann, L. H. Gamma- and Beta-Ray Hazards the Diagnosis of Early Radiation Injury. Transactions. *Conference on Metabolic Aspects of Convalescence* **1947**, *60*, 80−90.

(19) Chen, F.; Ehlerding, E. B.; Cai, W. Theranostic Nanoparticles. *J. Nucl. Med.* **2014**, *55*, 1919−1922.

(20) Chiang, S.-C.; Meagher, M.; Kassouf, N.; Hafezparast, M.; McKinnon, P. J.; Haywood, R.; El-Khamisy, S. F. Mitochondrial Protein-Linked DNA Breaks Perturb Mitochondrial Gene Transcription and Trigger Free Radical-Induced DNA Damage. *Sci. Adv.* **2017**, *3*, e1602506.

(21) Mao, F.; Wen, L.; Sun, C.; Zhang, S.; Wang, G.; Zeng, J.; Wang, Y.; Ma, J.; Gao, M.; Li, Z. Ultrasmall Biocompatible Bi2Se3 Nanodots for Multimodal Imaging-Guided Synergistic Radiophotothermal Therapy against Cancer. *ACS Nano* **2016**, *10*, 11145−11155.

(22) Horcajada, P.; Gref, R.; Baati, T.; Allan, P. K.; Maurin, G.; Couvreur, P.; Ferey, G.; Morris, R. E.; Serre, C. Metal-Organic Frameworks in Biomedicine. *Chem. Rev.* **2012**, *112*, 1232−1268.

(23) Rieter, W. J.; Pott, K. M.; Taylor, K. M. L.; Lin, W. Nanoscale Coordination Polymers for Platinum-Based Anticancer Drug Delivery. *J. Am. Chem. Soc.* **2008**, *130*, 11584.

(24) He, C.; Liu, D.; Lin, W. Nanomedicine Applications of Hybrid Nanomaterials Built from Metal-Ligand Coordination Bonds: Nanoscale Metal-Organic Frameworks and Nanoscale Coordination Polymers. *Chem. Rev.* **2015**, *115*, 11079−11108.

(25) He, C.; Liu, D.; Lin, W. Self-Assembled Core−Shell Nanoparticles for Combined Chemotherapy and Photodynamic Therapy of Resistant Head and Neck Cancers. *ACS Nano* **2015**, *9*, 991−1003.

(26) Liu, D. M.; Poon, C.; Lu, K. D.; He, C. B.; Lin, W. B. Self-Assembled Nanoscale Coordination Polymers with Trigger Release Properties for Effective Anticancer Therapy. *Nat. Commun.* **2014**, *5*. DOI: 10.1038/ncomms5182

(27) He, C. B.; Duan, X. P.; Guo, N. N.; Chan, C.; Poon, C.; Weichselbaum, R. R.; Lin, W. B. Core-shell Nanoscale Coordination Polymers Combine Chemotherapy and Photodynamic Therapy to Potentiate Checkpoint Blockade Cancer Immunotherapy. *Nat. Commun.* **2016**, *7*.12499
(28) Yang, Y.; Zhu, W.; Dong, Z.; Chao, Y.; Xu, L.; Chen, M.; Liu, Z. 1D Coordination Polymer Nanofibers for Low-Temperature Photothermal Therapy. *Adv. Mater.* **2017**, *29*, 29.
(29) Liu, J.; Yang, Y.; Zhu, W.; Yi, X.; Dong, Z.; Xu, X.; Chen, M.; Yang, K.; Lu, G.; Jiang, L.; Liu, Z. Nanoscale Metal-Organic Frameworks for Combined Photodynamic & Radiation Therapy in Cancer Treatment. *Biomaterials* **2016**, *97*, 1−9.
(30) Baeza, A.; Ruiz-Molina, D.; Vallet-Regi, M. Recent Advances in Porous Nanoparticles for Drug Delivery in Antitumoral Applications: Inorganic Nanoparticles and Nanoscale Metal-Organic Frameworks. *Expert Opin. Drug Delivery* **2017**, *14*, 783−796.
(31) Wang, C.; deKrafft, K. E.; Lin, W. Pt Nanoparticles@ Photoactive Metal-Organic Frameworks: Efficient Hydrogen Evolution via Synergistic Photoexcitation and Electron Injection. *J. Am. Chem. Soc.* **2012**, *134*, 7211−7214.
(32) Ma, Z.; Moulton, B. Recent advances of discrete coordination complexes and coordination polymers in drug delivery. *Coord. Chem. Rev.* **2011**, *255*, 1623−1641.
(33) Yang, Y.; Liu, J.; Liang, C.; Feng, L.; Fu, T.; Dong, Z.; Chao, Y.; Li, Y.; Lu, G.; Chen, M.; Liu, Z. Nanoscale Metal-Organic Particles with Rapid Clearance for Magnetic Resonance Imaging-Guided Photothermal Therapy. *ACS Nano* **2016**, *10*, 2774−2781.
(34) Zeng, J.-Y.; Zou, M.-Z.; Zhang, M.; Wang, X.-S.; Zeng, X.; Cong, H.; Zhang, X.-Z. π-Extended Benzoporphyrin-Based Metal−Organic Framework for Inhibition of Tumor Metastasis. *ACS Nano* **2018**.*1*24630
(35) Cheng, L.; Jiang, D.; Kamkaew, A.; Valdovinos, H. F.; Im, H.-J.; Feng, L.; England, C. G.; Goel, S.; Barnhart, T. E.; Liu, Z.; Cai, W. Renal-Clearable PEGylated Porphyrin Nanoparticles for Image-Guided Photodynamic Cancer Therapy. *Adv. Funct. Mater.* **2017**, *27*, 1702928.
(36) Huang, H.; Hernandez, R.; Geng, J.; Sun, H.; Song, W.; Chen, F.; Graves, S. A.; Nickles, R. J.; Cheng, C.; Cai, W.; Lovell, J. F. A Porphyrin-PEG Polymer with Rapid Renal Clearance. *Biomaterials* **2016**, *76*, 25−32.
(37) Butterworth, K. T.; McMahon, S. J.; Currell, F. J.; Prise, K. M. Physical Basis and Biological Mechanisms of Gold Nanoparticle Radiosensitization. *Nanoscale* **2012**, *4*, 4830−4838.
(38) Song, G.; Cheng, L.; Chao, Y.; Yang, K.; Liu, Z. Emerging Nanotechnology and Advanced Materials for Cancer Radiation Therapy. *Adv. Mater.* **2017**, *29*, 1700996.
(39) Song, G.; Liang, C.; Yi, X.; Zhao, Q.; Cheng, L.; Yang, K.; Liu, Z. Perfluorocarbon-Loaded Hollow Bi2Se3 Nanoparticles for Timely Supply of Oxygen under Near-Infrared Light to Enhance the Radiotherapy of Cancer. *Adv. Mater.* **2016**, *28*, 2716−2723.
(40) Kilian, K.; Pyrzynska, K. Tetrakis(p-carboxylphenyl)porphyrin as a Complexing Agent for Solid Phase Extraction of Metal Ions. *Chem. Anal-warsaw* **2002**, *47*, 439−447.
(41) Chao, Y.; Wang, G.; Liang, C.; Yi, X.; Zhong, X.; Liu, J.; Gao, M.; Yang, K.; Cheng, L.; Liu, Z. Rhenium-188 Labeled Tungsten Disulfide Nanoflakes for Self-Sensitized, Near-Infrared Enhanced Radioisotope Therapy. *Small* **2016**, *12*, 3967−3975.

DOI: 10.1021/acsnano.8b02400
ACS Nano 2018, 12, 7519−7528